J. Electrochem. Sci. Eng. **16** (2026) 3648; https://doi.org/10.5599/jese.3648

Open Access : : ISSN 1847-9286
https://pub.iapchem.org/ojs/index.php/JESE

Original scientific paper

Voltammetric determination of hydroxylamine using zinc ferrite nanoparticles/Mn(III) salen-doped carbon paste electrode

Rasha M. Dadoosh[1,✉], Athraa H. Oraibi[2], Noor Faraj Kadhem[2], Sabaa Abd Jaber[3] and Muntaha Harjan Elewi[4]

[1]*Chemistry Department, College of Science, Mustansiriyah University, Baghdad, Iraq*
[2]*Polymer Research Unit, College of Science, Mustansiriyah University, Baghdad, Iraq*
[3]*College of Engineering, Al-Iraqia University, Baghdad, Iraq*
[4]*Scientific Research Commission, Baghdad, Iraq*

Corresponding Author: ✉*rashamunim@uomustansiriyah.edu.iq*

Received: July 23, 2026; Accepted: September 21, 2026; Published: November 1, 2026

Abstract

Modification of carbon paste electrode (CPE) with $ZnFe_2O_4$ nanoparticles and Mn(III) salen (ZFO/salen/CPE) and its application in the measurement of hydroxylamine (HX) are the topics of this work. Differential pulse voltammetry, chronoamperometry and cyclic voltammetry (CV) were used in the investigations of the ZFO/salen/CPE for the electrochemical analysis of hydroxylamine. Because of the synergistic effect of the Mn(III) salen and $ZnFe_2O_4$ nanoparticles, the CV analyses showed improved catalytic behaviour of ZFO/salen/CPE toward the electrochemical reaction of HX. The linear range and HX detection limit were found to be 50 nM to 0.30 mM and 20 nM, respectively, using SWV. Long-term stability and reproducibility were demonstrated by this sensor. To confirm the sensor's appropriateness for use, HX measurement in water samples was carried out.

Keywords

Voltammetry; chemically modified electrode; water analysis; environmental pollution

Introduction

Ammonia's inorganic constituent, hydroxylamine (HX), participates in a variety of oxidation and reduction processes. Nuclear fuel reprocessing, semiconductor manufacturing, and pharmaceutical intermediates are just a few of the many uses for HX [1]. It is also involved in several biological processes, including acting as a vasodilator in the rat kidney's blood vessels, suppressing insulin release, activating K+ channels, and serving as an intermediate in converting L-arginine to nitric oxide in cellular metabolism [1].

HX is a mutation agent that is relatively toxic, causing both repairable and irreversible physiological changes in the organs of humans, mammals, and plants [2]. It can also irritate the skin, eyes, mucous

membranes, and respiratory pathways. Long-term exposure to HX can also cause skin allergies and blood changes, including methemoglobin formation, which over time may induce anaemia and glutathione depletion. Additionally, when heated, HX may explode [3], and through cytochrome P460, HX can transform into nitrous oxide [4].

Some analytical methods are used in recent years to detect HX [5]. Today, electrochemical methods are more dependable and widely used than other methods and have been extensively considered for studying a variety of materials because of their many benefits, including increased sensitivity and selectivity, faster determination, and lower cost [5].

CPEs are used as electrochemical sensors because of their ease of fabrication, surface renewability, low cost and ability to be modified with different types of modifiers. Modifying electrodes with different modifiers improves detection limits, sensitivity, overpotential, and resistance to surface fouling [6,7]. Nanoparticles' special chemical and physical characteristics make them ideal for electrode modification. Electrochemical sensors and biosensors have been built using a variety of nanomaterials [8].

The biomedical and pharmaceutical industries have made extensive use of electrochemical nanosensors, which have many advantages over other sensors and techniques, including high sensitivity, a wider linear response range, low detection limits, and good reproducibility and stability. Today, environmental, pharmaceutical, and clinical laboratories, as well as commercial point-of-care devices, use a variety of analytical methods that incorporate nanosensors to some degree [9].

Currently, a variety of nanoparticles are frequently used as modifiers in sensor construction; however, because of their reduced Zn^{2+} toxicity, zinc ferrite nanoparticles have drawn interest in the field of nano-medicine. Because current contrast agents are more hazardous, this is particularly desirable for magnetic resonance imaging (MRI) contrast agents. $ZnFe_2O_4$ nanoparticles (ZFO) are a good choice for MRI contrast agents since their RDI (reference daily intake) permitted levels are suitable. Compared to other biocompatible materials, this is significantly higher [10,11].

The electrode/solution interface is where electrochemical nanosensors detect signals [12,13].

No study utilizing ZFO/salen/CPE for electrocatalytic HX determination has been published to date. Therefore, the fabrication and applicability of ZFO/salen/CPE for measurement of HX were first discussed in this study. The improved electrode's analytical performance in measuring HX in actual samples was then assessed.

Experimental

Apparatus and chemicals

An Autolab potentiostat/galvanostat (PGSTAT 12N, Netherlands) was used to conduct the electrochemical measurements. The reference, auxiliary, and working electrodes were Ag/AgCl/KCl, platinum wire, and ZFO/salen/CPE, respectively. Every solution was made fresh using double-distilled water. Merck (Darmstadt, Germany) supplied the analytical-grade hydroxylamine and all other reagents. Orthophosphoric acid and its salts in the pH range of 2.0 to 9.0 were used to create the buffer solutions (PBS).

Synthesis of $ZnFe_2O_4$ nanoparticles

$ZnFe_2O_4$ nanoparticles were synthesized by coprecipitation. In brief, 250.2 g of $ZnCl_2{\cdot}4H_2O$ and 570.5 g of $FeCl_3{\cdot}6H_2O$ were dissolved simultaneously in 200 mL of water in a 250 mL double-necked volumetric flask. The two mixtures were heated in an oil bath at 80 °C for 6 h under a nitrogen atmosphere. During the reaction period, 50 mL of 6 M NaOH was added slowly to the final solution.

(cc) BY

After a few minutes, the first precipitates, linked to the formation of $ZnFe_2O_4$ nanoparticles, began to nucleate. The precipitates were washed multiple times with distilled water to remove extraneous residues and impurities. Next, the suspension was centrifuged to separate the precipitates formed during $ZnFe_2O_4$ nanoparticle formation. Finally, to remove remaining impurities, the products were dried in an oven at 60 °C for 24 hours.

Preparation of the electrode

To determine the best composition for ZFO/salen/CPEs, we optimized the amount of Mn(III) salen, and $ZnFe_2O_4$ nanoparticles used together. The highest current of HX was obtained at ZFO/salen/CPE when the ratio of Mn(III) salen to $ZnFe_2O_4$ nanoparticles was properly balanced. The ZFO/salen/CPEs were made by adding 0.02 g of Mn(III) salen to 0.94 g graphite, 0.04 g $ZnFe_2O_4$ and 0.8 mL of paraffin. It was stirred for 15 min. The resulting paste was packed in a glass tube. If needed, a fresh surface was prepared by pushing out more paste from the tube and polishing. For comparison, salen/CPEs without $ZnFe_2O_4$ nanoparticles, ZFO/salen/CPE without Mn(III) salen, and also an unmodified CPE in which neither Mn(III) salen nor $ZnFe_2O_4$ nanoparticles were present were prepared in the same way.

Preparation of the real samples

Based on the research design, we used multiple drinking water samples and tap water (from the laboratory) as the real or reference samples. After that, the water samples were filtered. Different amounts of HX were added to the water samples and they were examined.

Results and discussion

Electrochemical properties of zinc ferrite nanoparticles/Mn(III) salen-doped carbon paste electrode

Cyclic voltammetry (CV) in PBS at pH 7 was used to examine the electrochemical characteristics of Mn(III) salen. The insolubility of Mn(III) salen in aqueous media is one of its benefits as an electrode modifier. The experiments demonstrated reproducible and distinct CVs. The cathodic peak potential (E_{pc}) was 0.53 V, while the anodic peak potential (E_{pa}) was 0.64 V (Figure 1).

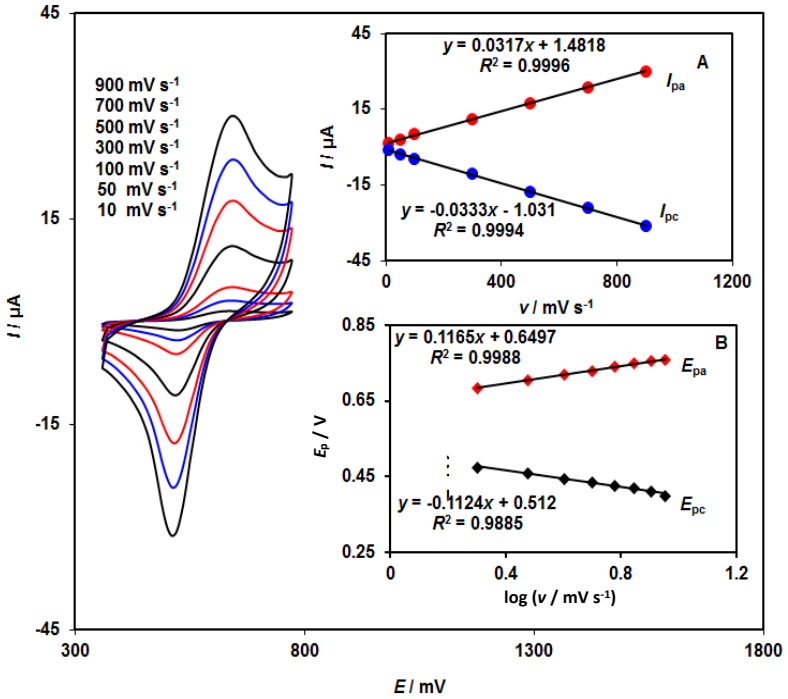


Figure 1. *The CVs of ZFO/salen/CPE in PBS at different scan rates. The insets show variations in (A)* I *versus scan rate and (B)* E_p *versus the logarithm of the high scan rate*

CV was also used to examine the impact of the scan rate (v) on electrochemical characteristics of the ZFO/salen/CPE. Plots of peak currents (I_p) in the range of 10 to 900 mV s^{-1} were linearly dependent on v (Figure 1A), suggesting that the Mn(III) salen redox process at the ZFO/salen/CPE is consistent with that expected for a surface-confined redox pair.

According to Laviron's method [14], the variation of E_{pa} and E_{pc} with the log v can be used to determine the apparent charge-transfer rate constant, k_s, and the charge-transfer coefficient, α. These plots are shown in Figure 1B, which indicates that for $v > 2$ V s^{-1}, the E_{pa} and E_{pc} values are proportional to log v. α_c and α_a can be extracted from the slopes in Figure 1B. For the cathodic and anodic peaks, the slope of the linear segments is equal to -2.303RT/αnF and 2.303RT/(1–α)nF, respectively. The α has an assessed value of 0.5.

Additionally, k_s between Mn(III) salen and ZFO/CPE may be found using Equation (1). Using Equation (1), the value of k_s was determined to be 15.1 s^{-1}.

$$\log k_s = \alpha \log (1-\alpha) + (1-\alpha) \log \alpha - \log (RT/nFv) - \alpha (1-\alpha) nF\Delta E_p/2.3RT \quad (1)$$

Furthermore, a three-week interval was used to examine the ZFO/salen/CPE's long-term stability. The potential for HX oxidation remained intact, and the current exhibited less than a 2.1 % drop compared to the initial response when CVs were measured during ZFO/salen/CPE's storage in the environment.

By measuring the modified electrode's cyclic voltammograms before and after use in the presence of HX, the antifouling characteristics of ZFO/salen/CPE toward HX were examined. After cycling the potential 15 times, CVs were collected in the presence of HX. The currents dropped by less than 2.3 %, while the peak potentials remained constant. The fouling effect of the analyte diminished at the ZFO/salen/CPE.

Cyclic voltammetric data collected at the optimum solution pH of 7.0 from five independently constructed ZFO/salen/CPEs were used to assess the electrode's potential to produce a repeatable surface. The computed RSD for several parameters is considered the standard for suitable surface repeatability (about 1 to 4 %), which is essentially the same as what is expected for a renewed or regular CPE.

Electrocatalytic oxidation of hydroxylamine at zinc ferrite nanoparticles/Mn(III) salen-doped carbon paste electrode

Because it affects the electrochemical behaviour, pH adjustment is necessary. Therefore, the electrochemical behaviour of HX at ZFO/salen/CPE was investigated using CV in 0.1 M PBS at various pH values from 2.0 to 8.0. It was discovered that neutral conditions were more favourable for oxidation of HX at the ZFO/salen/CPE. The ideal pH was therefore determined to be 7.0.

The CV responses for 30.0 µM HX at unmodified CPE, ZFO/CPE, salen/CPE and ZFO/salen/CPE are shown in Figure 2. Additionally, curve a displays unmodified CPE in PBS. As can be shown, the potential at ZFO/salen/CPE and salen/CPE is around 640 mV, but for ZFO/CPE and unmodified CPE, it is 990 and 1040 mV.

In comparison to ZFO/CPE and unmodified CPE, these results show that Mn(III) salen can function as a good mediator and that the potential of ZFO/salen/CPE and salen/CPE shifts by 350 and 400 mV, respectively. However, compared with salen/CPE, ZFO/salen/CPE shows a substantially higher current for HX oxidation, suggesting that combining ZFO with the mediator (Mn(III) salen) greatly enhances the electrode's performance for HX oxidation. In fact, ZFO/salen/CPE showed a well-behaved redox reaction in PBS without HX (Figure 2, curve c). In the presence of HX, the current increased dramatically (curve f), which may be attributed to the ZFO/salen/CPE's strong electro-catalytic activity toward HX.

(cc) BY

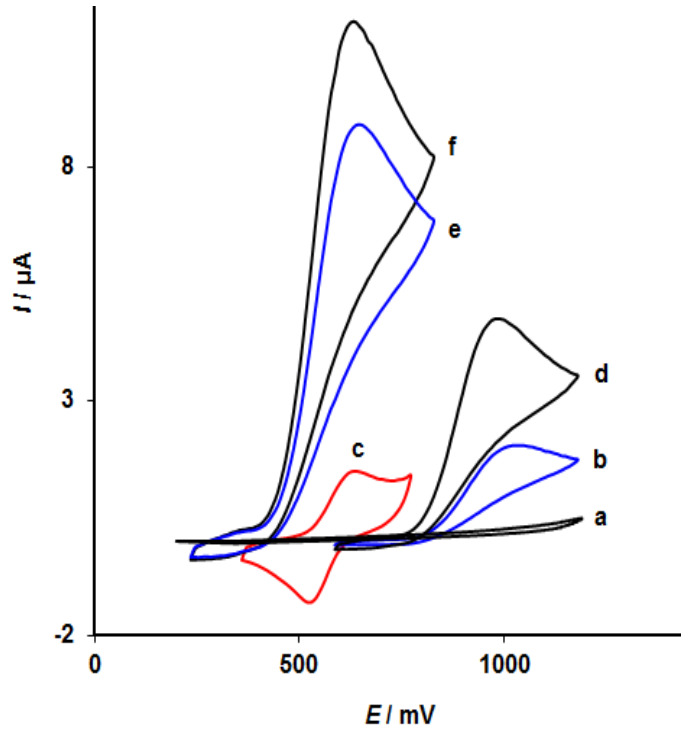


Figure 2. *The CVs for (a) unmodified CPE in PBS, (b) unmodified CPE in 30.0 µM HX, (c) ZFO/salen/CPE in PBS, (d) ZFO/CPE in 30.0 µM HX, (e) salen/CPE in 30.0 µM HX and (f) ZFO/salen/CPE in 30.0 µM HX. The scan rate was 10 mV s^{-1} in every instance*

CV was used to examine the impact of scan rate on the electrocatalytic oxidation of HX at the ZFO/salen/CPE (Figure 3). A plot of current *vs.* the square root of scan rate ($v^{1/2}$) was linear, indicating that the process is diffusion-controlled at adequate overpotential (Figure 3A). The usual shape of an EC process may be seen in a plot of the scan rate-normalized current ($I/v^{1/2}$) *vs. v* (Figure 3B).

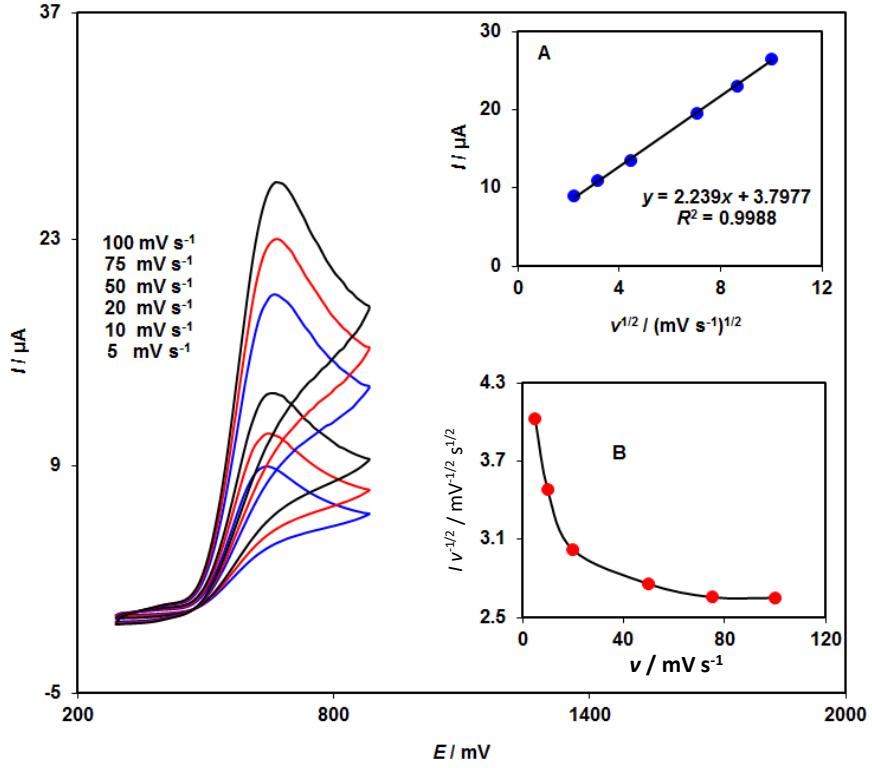


Figure 3. *CVs of ZFO/salen/CPE at different scan rates in PBS containing 30.0 µM HX. Variations of (A)* I vs. $v^{1/2}$ *and (B)* ($I/v^{1/2}$) vs. v

Chronoamperometric studies

The current-time curves obtained for HX at ZFO/salen/CPE by adjusting the potential to 1020 mV are shown in Figure 4A. The Cottrell Equation (2) is used to determine the diffusion coefficient (D):

$$I=nFAD^{1/2}C_b\pi^{-1/2}t^{-1/2} \quad (2)$$

where D / cm^2 s^{-1} and C_b / mol cm^{-3} are the diffusion coefficient and the bulk concentration, respectively. Figure 4B shows the experimental plots for different concentrations of HX. The D was found to be 0.00000755 cm^2 s^{-1} using the slope in Figure 5A.

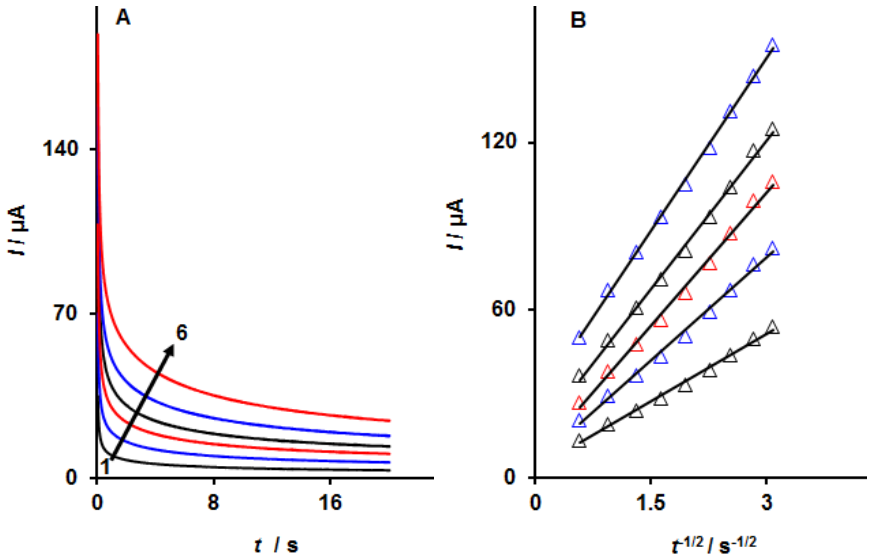


Figure 4. *(A) Chronoamperograms for various HX concentrations measured at ZFO/salen/CPE in PBS. (B)* I vs. $t^{-1/2}$ *plots*

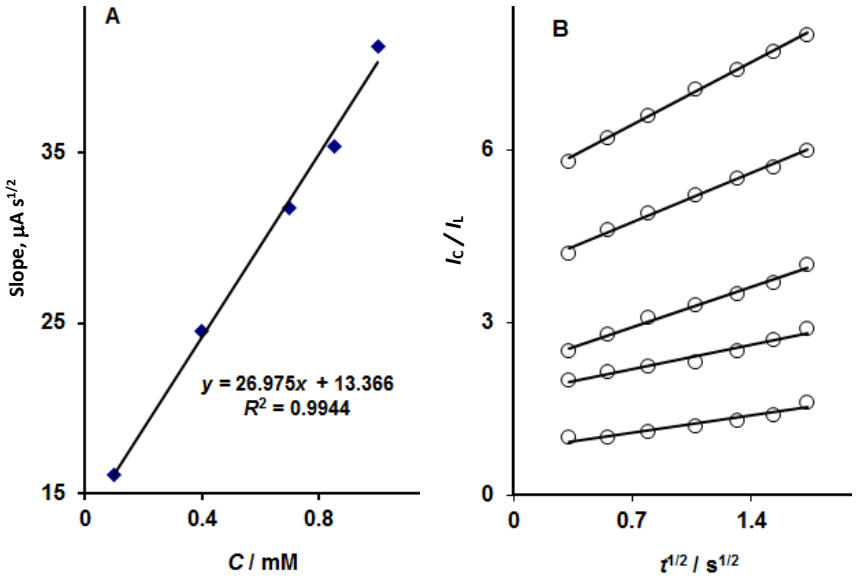


Figure 5. *(A) Plot of the slope versus HX concentration. (B)* I_C/I_L *dependence on* $t^{1/2}$

Chronoamperometry can be employed to evaluate the catalytic rate constant (k_h), according to the method of Galus [15]:

$$I_C/I_L = \gamma^{1/2}[\pi^{1/2}\,\mathrm{erf}\,\gamma^{1/2} + \exp(-\gamma/\gamma^{1/2})] \quad (3)$$

where $\gamma = k_hC_bt$ is the argument of the error function, I_C is the catalytic current of HX at ZFO/salen/CPE, and I_L is the limiting current in the absence of HX. When γ is greater than two, the error function is nearly equal to 1, hence, the equation above can be simplified to Equation (4):

$$I_C/I_L = \pi^{1/2}\gamma^{1/2} = \pi^{1/2}(kC_bt)^{1/2} \quad (4)$$

(cc) BY

where t is the time elapsed in seconds. The catalytic process's rate constant, k_h, can be computed using the formula above. For a particular HX concentration, k_h can be found using the slope of the I_C/I_L *vs.* $t^{1/2}$ plot (Figure 5B). Thus, k_h was determined to be $k_h = 1.38\times10^3$ $M^{-1}s^{-1}$.

Calibration plot and limit of detection

The concentration of HX was measured using DPV (Figure 6). Two linear segments in the ranges of 0.05 to 30.0 µM and 30.0 to 300.0 µM, respectively, made up the plot of peak current *vs.* HX concentration. Kinetic constraints likely caused the decreased sensitivity (slope) of the second linear segment. The HX detection limit was 0.02 µM.

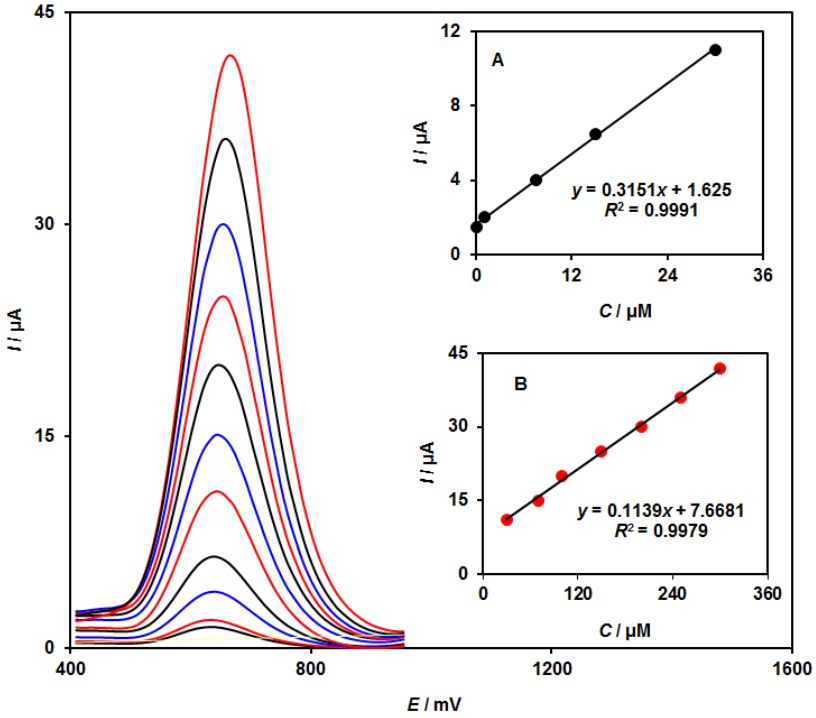


Figure 6. *DPVs of ZFO/salen/CPE in PBS with varying HX concentrations. Plots of I vs HX concentration in the range of 0.05 to 30.0 µM (A) and 30.0 to 300.0 µM (B) are displayed in the insets*

Analysing the real samples

At this point, the current technique was used to measure HX in water samples to assess the usefulness of ZFO/salen/CPE to measure HX in actual samples. We also used the normal addition procedure. The obtained results are shown in Table 1. Additionally, excellent HX recoveries were obtained, demonstrating repeatable results based on the mean relative standard deviation (RSD).

Table 1. *HX concentration measurement in water samples (n = 5)*

Sample	Amount, µM		Recovery, %	RSD, %
	Spiked	Found		
Drinking water	5.0	5.1	102.0	3.2
	7.0	6.8	97.1	2.4
	9.0	8.9	98.9	2.9
	11.0	10.9	99.1	1.7
River water	5.5	5.3	96.4	2.3
	7.5	7.6	101.3	3.1
	9.5	9.4	98.9	1.9
	11.5	12.0	104.3	2.0

Conclusion

By using ZFO and salen in ZFO/salen/CPE, a sensor was developed to determine HX. The results showed that HX oxidation catalysis occurs at pH 7.0 and that the peak potential of HX shifts by 400 mV at the modified electrode. With a 0.01 µM HX detection limit, DPV shows linearity over a dynamic range of 50 nM to 0.30 mM. Finally, ZFO/salen/CPE was studied as a novel electrochemical sensor for measuring HX in actual specimens and was found to be precise, easy to use and selective.

Funding: *Not applicable.*

Conflict of interest*: None.*

References

[1] U. K. Deogratias, D. Jin, X. Zhang, N. A. H. Forde, G. Y. Bhrane, M. A. Jalloh, P. Wu, Double-edged effects and regulation mechanism of hydroxylamine in novel nitrogen removal processes: A comprehensive review, *Journal of Water Process Engineering* **69** (2025) 106826. https://doi.org/10.1016/j.jwpe.2024.106826

[2] E. Freese, E. Bautz-Freese, E. Bautz, Hydroxylamine as a mutagenic and inactivating agent, *Journal of Molecular Biology* **3** (1961) 133-143. https://doi.org/10.1016/S0022-2836(61)80040-5

[3] M. K. F. Wikström, Inhibition of oxidative phosphorylation by hydroxylamine in sonicated particles from beef-heart mitochondria, *Biochimica et Biophysica Acta (BBA) - Bioenergetics* **234** (1971) 16-27. https://doi.org/10.1016/0005-2728(71)90124-1

[4] M. A. Smith, S. H. Majer, A. C. Vilbert, K. M. Lancaster, Controlling a burn: outer-sphere gating of hydroxylamine oxidation by a distal base in cytochrome P460, *Chemical Science* **10** (2019) 3756-3764. https://doi.org/10.1039/c9sc00195f

[5] M. Nazari, H. Asadollahzadeh, M. Shahidi, N. Rastakhiz, S.Z. Mohammadi, Sensitive determination of hydroxylamine by using modified electrode by La_2O_3-Co_3O_4 nanocomposite and ionic liquid, *Materials Chemistry and Physics* **286** (2022) 126209. https://doi.org/10.1016/j.matchemphys.2022.126209

[6] I. Eskandary, Mo. R. Baezzat, N. Tavakkoli, N. Soltani, Electrochemical Measurement of Tramadol Using a Sensor Modified with PdNP@Al_2O_3 Nanocomposite in the Presence of Morphine, *Analytical and Bioanalytical Chemistry Research* **13** (2026) 33-47. https://doi.org/10.22036/abcr.2025.531074.2376

[7] E. M. Alemán-Luna, C. S. Gómez-Navarro, C. D. Patiño-Arévalo, Y. A. Guerrero-Cobos, M. A. Zárate-Navarro, A. I. Zárate-Guzmán, L. A. Romero-Cano, Carbon paste electrode-based electroanalytical method for electrochemical fingerprinting of flavored agave syrups, *Food Chemistry* **505** (2026) 147962. https://doi.org/10.1016/j.foodchem.2026.147962

[8] N.Soltani, N. Ziaie, N. Tavakkoli, E. Eslami, CdS Nanoparticles and Schiff Base-modified CPE for Simultaneous Determination of Dopamine, Ascorbic Acid, and Uric Acid, *Analytical and Bioanalytical Chemistry Research* **13** (2026) 105-118. https://doi.org/10.22036/abcr.2025.549005.2428

[9] P. Bhatt, M. Chhillar, A. Singh, D. Kukkar, A. Kumar, A. K.Yadav , J. Kaur, M. Kukkar, Electrochemical nanosensors using MXene-carbon dot modified screen-printed carbon electrodes for creatinine detection in serum samples, *Materials Advances* 7 (2025) 277-288. https://doi.org/10.1039/d5ma00539f

[10] F. de J. Silerio-Vázquez, R. Dewil, L. Chaabane, B.L. Su, B. Kakavandi, J. B. Proal-Nájera, Critical insights on progress and prospects for emerging contaminants photocatalytic degradation with zinc ferrite ($ZnFe_2O_4$) heterojunctions, *Sustainable Materials and Technologies* **47** (2026) e01816. https://doi.org/10.1016/j.susmat.2025.e01816

(cc) BY

[11] I. D. Shabalkin, A. S. Komlev, S. A. Tsymbal ,O. I. Burmistrov ,V. I. Zverev, P. V. Krivoshapkin, Multifunctional tunable $ZnFe_2O_4$@$MnFe_2O_4$ nanoparticles for dual-mode MRI and combined magnetic hyperthermia with radiotherapy treatment, *Journal of Materials Chemistry B* **11** (2023)1068-1078. https://doi.org/10.1039/d2tb02186b

[12] E. Kipkorir, O. Kimani, Electrochemical sensing of pharmaceutical pollutants using modified glassy carbon electrodes with nanostructures: A review, *Inorganic Chemistry Communications* **179** (2025) 114827. https://doi.org/10.1016/j.inoche.2025.114827

[13] N. N. Mohamad Zain, N. Yahaya, Kartika A. Madurani, S. Shahabuddin, K. P. Sambasevam, S. N. Atika Baharin, I. Jeerapan , Green techniques: Revolutionizing deep eutectic solvents-based modified electrodes for electrochemical sensing of natural antioxidant, *Microchemical Journal* **206** (2024) 111491. https://doi.org/10.1016/j.microc.2024.111491

[14] E. Laviron, General expression of the linear potential sweep voltammogram in the case of diffusionless electrochemical systems, *Journal of Electroanalytical Chemistry and Interfacial Electrochemistry* **101** (1979) 19-28. https://doi.org/10.1016/S0022-0728(79)80075-3

[15] Z. Galus, *Fundamentals of Electrochemical Analysis*, Ellis Horwood, New York, 1976. ISBN 0470150807

©2026 by the authors; licensee IAPC, Zagreb, Croatia. This article is an open-access article distributed under the terms and conditions of the Creative Commons Attribution license (http://creativecommons.org/licenses/by/4.0/)